J Mater Sci (2007) 42:2551–2556
DOI 10.1007/s10853-006-1230-1

Synthesis, crystallographic characterization and ionic conductivity of iron substituted sodium zirconium phosphate $Na_{1.2}Zr_{1.8}Fe_{0.2}(PO_4)_3$

O. P. Shrivastava · Narendra Kumar · Rashmi Chourasia

Received: 7 August 2005 / Accepted: 23 January 2006 / Published online: 2 January 2007

Sodium zirconium phosphate $NaZr_2P_3O_{12}$ (hereafter NZP) crystallizes in rhombohedral (hexagonal) symmetry with the space group *R*-3c. The NZP-related phase of synthetic iron substituted NZP has been prepared by partial substitution on zirconium site by Fe(III). The material has been synthesized by sintering the finely powdered oxide mixture in a muffle furnace at 1,050 °C. The polycrystalline phase of $Na_{1.2}Zr_{1.8}Fe_{0.2}(PO_4)_3$ has been characterized by its typical powder diffraction pattern. The powder diffraction data of 3,000 points have been subjected to general structural analysis system (GSAS) software to arrive at a satisfactory structural fit with $R_p = 0.0623$ and $R_{wp} = 0.0915$. The following unit cell parameters have been calculated: $a = b = 8.83498(18)$ Å, $c = 22.7821(8)$ Å and $\alpha = \beta = 90.0°$ $\gamma = 120.0°$. The structure of NZP consists of ZrO_6 octahedra and PO_4 tetrahedra linked by the corners to form a three-dimensional network. Each phosphate group is on a two-fold rotation axis and is linked to four ZrO_6 octahedra. Each zirconium octahedron lies on a threefold rotation axis and is connected to six PO_4 tetrahedra. AC conductivity of the solid solution has been measured between 303 and 773 K. The material exhibits temperature-dependent enhancement of ionic conduction by ≈400 times at elevated temperatures. The activation energies show significant change in slope at $1{,}000/T = 2.23$(448 K).

O. P. Shrivastava (✉) · N. Kumar · R. Chourasia
Department of Chemistry, Dr. H. S. Gour University, Sagar 470 003, India
e-mail: dr_ops11@rediffmail.com

Introduction

Materials of sodium zirconium phosphate (NZP) family have attracted wide interest due to their ability to immobilize radioactive nuclides from intermediate level nuclear waste [1–3]. A new concept for converting the intermediate level nuclear waste resulting from light water reactor (LWR) fuel reprocessing in to a single phase material has been established. Low thermal expansion [4, 5], high ionic conduction and possible catalytic properties [6–8] also make such materials interesting. The standard formula for NZP group of materials is described as $[M'_1][M''_2][A^{IV}{}_2][X^{IV}{}_3]O_{12}$ where M′ and M″ are the two interstitial sites. A^{IV}, an octahedral site is normally occupied by Zr^{4+}. The X^{IV} site is a tetrahedral one occupied by P^{5+}. In this context several new phases have been identified on account of the interaction of NZP with several radwaste cations [9]. This immobilization process takes place through substitution for Na^+ on M′ site, Zr^{4+}on A site and P^{5+} on X site. Though some of the new phases of NZP-related materials have been identified by preliminary X-ray diffraction data but a systematic approach towards the structure property relationship is desirable to demonstrate the fundamental technical feasibility of this concept.

In rhombohedral polycrystalline NZPs, the PO_4 tetrahedra are linked with ZrO_6 octahedra by corner sharing, hence forming a three-dimensional framework with $[Zr_2(PO_4)_3]^-$ where each O atom is bonded to only one P and one Zr atom. The columns of three units lie along *c* direction running in hexagonal unit cell parallel to each other. These columns are inter linked through PO_4 tetrahedra in the direction perpendicular to *c*-axis to develop a three-dimensional

framework of columns which are capable to accommodate the larger alkali cations. NZP structures have two kinds of hole, one alkali site occurs in the column of Zr octahedra (M_1) and the other site (M_2) located between columns of Zr octahedra. Former is usually occupied, whereas the later is vacant. This M_2 site can be populated by additional cations, which compensate the charge with polyvalent cations other than zirconium [10].

It is also known that materials with ''Nasicon'' type structure are in general good ionic conductors due to the presence of channels in which alkali ions can move easily [11]. The family of NZP materials has been recognized as a three-dimensional Na^+ ionic conductor with framework structure and they are important in the sense that they have Na^+ ionic conductivity of the high order of magnitude. The structural framework of NZP is built up of two ZrO_6 octahedra and three PO_4 tetrahedra, sharing corners such that every oxygen belongs simultaneously to a tetrahedron and an octahedron [12, 13]. The Na^+ ions occupy a site with an octahedral oxygen environment between two $Zr_2(PO_4)_3$ units at the intersection of three conduction channels (M_1 site). The M_2 site becomes populated when additional cations needed for charge compensation with polyvalent cations other than zirconium. The framework and the ions inserted into M_1 and M_2 sites behave as two parts of the structure playing different role. Both sites are arranged in an alternating manner along the conduction channels [14, 15]. In this communication we report Rietveld refinement of crystallographic data and AC conductance behavior of phase pure polycrystalline iron substituted NZP ($Na_{1.2}Zr_{1.8}Fe_{0.2}(PO_4)_3$).

Experimental

Synthesis of the title phase of iron substituted NZP has been carried out as follows: calculated quantities of sodium, zirconium, iron and phosphorous corresponding to the molecular formula $Na_{1.2}Zr_{1.8}Fe_{0.2}(PO_4)_3$ have been thoroughly grinded to a fine powder in glycerol medium using mortar and pestle. AR quality Na_2CO_3, $ZrO(NO_3)_2 \times H_2O$, $Fe(NO_3)_3.6H_2O$ and $NH_4H_2PO_4$ were used in appropriate quantities as source of Na, Zr, Fe and P, respectively. The oxide route solid-state synthesis of ceramic phase was carried out by repeated grinding, palletizing and sintering the glycerol paste at 1,050 °C. After 72 h of sintering, densification of the material took place and a polycrystalline solid solution was formed. Powder X-ray diffractogram was recorded on a Rigaku Multiflex diffractometer at room temperature by step scanning from 10–80° 2θ in increments of 0.02° (0.2°/min) and a counting rate of 6 s/step.

Electrical conductivities have been determined by AC impedance spectroscopy. Measurements were carried out using HIOKI LCR HITESTER 3532-50. The frequency range from 42 Hz to 5 MHz was investigated. Impedance data were collected in the range of ambient temperature to 500 °C over heating and cooling cycles. Samples for electrical measurements were prepared as 1.29 cm diameter pellets of 0.333 cm thickness. Electrodes were applied using Ag paint.

Results and discussion

Structure refinement

The iron substituted NZP is light brown in colour. The colour intensity depends on Fe content. The intensities and positions of the diffraction pattern of the title phase matched fairly with the standard pattern of parent NZP which gives characteristics intense lines at 2θ = 19.467, 20.172, 23.363, 28.176 and 31.124 (Fig. 1) [16]. The step scan data of 3,000 points has been subjected to general structure analysis system (GSAS) programming [17]. The Rietveld refinement of the phase was performed by the least square method. The refinement shows a convergence to a satisfactory structure fit giving $R_p = 0.0623$ and $R_{wp} = 0.0915$ (Table 1). The cell parameters a and c are slightly greater than the corresponding cell parameters of

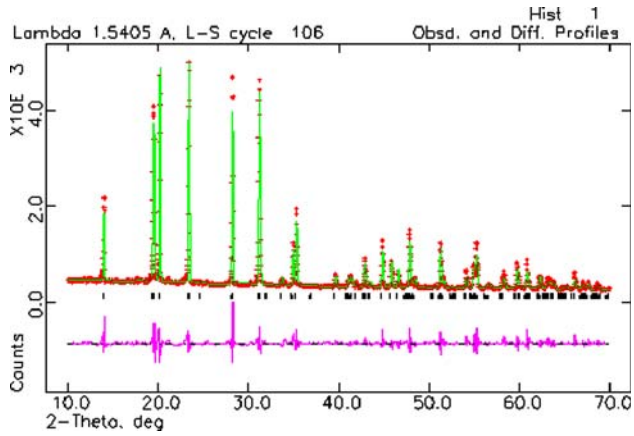

Fig. 1 Rietveld refinement pattern of $Na_{1.2}Zr_{1.8}Fe_{0.2}(PO_4)_3$. The '+' are the raw X-ray diffraction data, and the overlapping *continuous line* is the calculated pattern. *Black vertical* lines in the profile indicate the position of the allowed reflections for CuKα1 and CuKα2. The *curve* at the *bottom* is the difference in the observed and calculated intensities in the same scale

Table 1 Crystallographic data for $Na_{1.2}Zr_{1.8}Fe_{0.2}(PO_4)_3$ at room temperature

Structure	Rhombohedral
Space group	*R*-3c
Lattice parameters	a = 8.83498(18) Å
	b = 8.83498 Å
	c = 22.7821(8) Å
	$\alpha = \beta$ = 90.0
	γ = 120.0
Z	6
R_{wp}	9.15%
R_p	6.23%
R expected	4.68%
Volume of unit cell	1,540.05(5) Å^3
Density_{cal}	3.34 g/cm^3
Density_{exp}	3. 20 g/cm^3

$$R_p = \frac{\sum y_i(\text{obs}) - y_i(\text{cal})}{\sum y_i(\text{obs})} \qquad R_{wp} = \left\{ \frac{\sum w_i [y_i(\text{obs}) - y_i(\text{cal})]^2}{\sum w_i (y_i(\text{obs}))^2} \right\}^2$$

$$R_e = \left[(N - P) / \sum w_i y_{oi}^2 \right]^{1/2}$$

N number of observations, P number of parameters adjusted

$NaZr_2(PO_4)_3$. The cell volume is also increased by around 9 Å^3. Alteration in the lattice parameters of rhombohedral NZP compound shows that the network modifies its dimension to adapt to the size of the cation occupying M_1 and M_2 site without breaking the bonds. The basic framework may accept cations having different sizes and oxidation degrees into its holes, and at the same time the solid solution retains considerably its overall geometry. The final coordinates (Table 2), interatomic distances (Table 3) bond angles and structure factors (Appendices 1, 2) are extracted from the crystal information file (CIF) prepared by the software. The absences of the reflection of the type $h - k + l = 3n$ unambiguously indicate the R lattice. The values of Zr–O, P–O bond lengths match with their standard values [18]. The crystal structure of the title phase may be described in terms of constituent PO_4 tetrahedra and ZrO_6 octahedra which are linked by corners to form a three-dimensional network. The PO_4 tetrahedra are nearly regular (Fig. 2). The P–O distances 1.64 Å and 1.53 Å are

Table 2 Final atomic coordinate of $Na_{1.2}Zr_{1.8}Fe_{0.2}(PO_4)_3$ at room temperature

Name	x	y	z	Occupancy	Uiso
Na1	0	0	0	1.06485	0.19359
Na2	0.05765	0.37398	0.11257	0.0695	0.28881
Zr3	0	0	0.14559	0.79812	0.067
Fe4	0	0	0.14559	0.20188	0.09
P5	0.28261	0	0.25	1	0.08465
O6	0.17702	–0.04138	0.19278	1.0512	0.09047
O7	0.19016	0.15762	0.08887	1.03482	0.08697

Table 3 Interatomic distances (Å) of polycrystalline $Na_{1.2}Zr_{1.8}Fe_{0.2}(PO_4)_3$

P5	O7	1.643490(30) × 2
P5	O6	1.53690(4) × 2
Zr3	O6	2.07537(4) × 3
Zr3	O7	2.02301(4) × 3
Na2	O6	2.24770(5)
Na2	O6	2.45362(5)
Na2	O7	2.74842(5)
Na2	O7	2.69656(5)
Na2	O7	2.49343(5)
Na2	O7	2.17814(4)

comparable to those found by Cruickshank and Nord [19, 20]. The ORTEP view generated by the refined structural data shows that in the Zr–O bonds are in three pairs resulting in six coordination of zirconium. The Zr–O bond lengths are obtained in two sets 2.07 and 2.02 Å. The planer O–Zr–O angles are different from those connecting the apex oxygen atoms of the octahedron (Fig. 4). The O6–Zr–O7 bond angle in the ORTEP is 171.4492 indicating that the ZrO_6 octahedra are slightly tilted (Fig. 3). The other O–Zr–O angle values occur in triplicate (Appendix 1).

Electrical conductivity

The conductivity of the solid electrolyte stems from ionic conduction i.e. migration of ionic species, (mostly Na^+ in this case) and electronic conductivity (movement

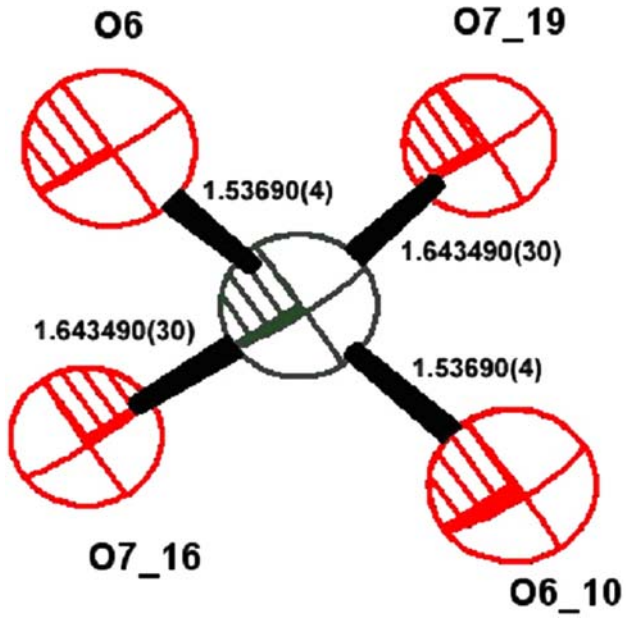

Fig. 2 ORTEP view of phosphorous coordination in PO_4 tetrahedra

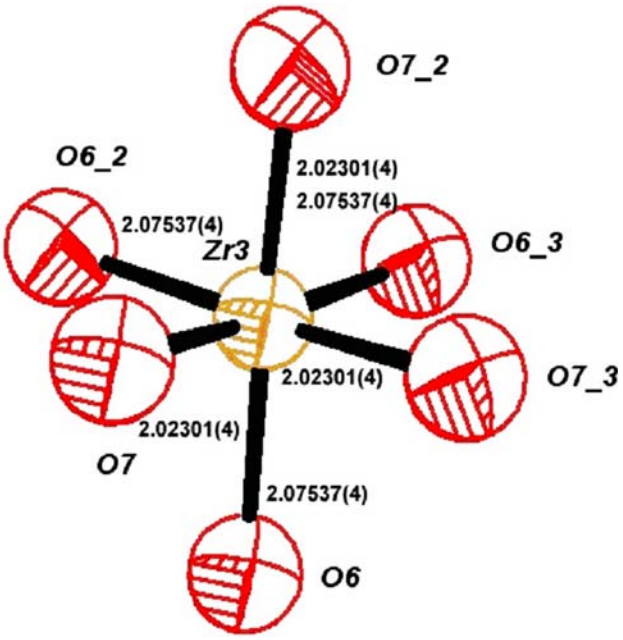

Fig. 3 ORTEP view of Zr coordination in ZrO_6 octahedra

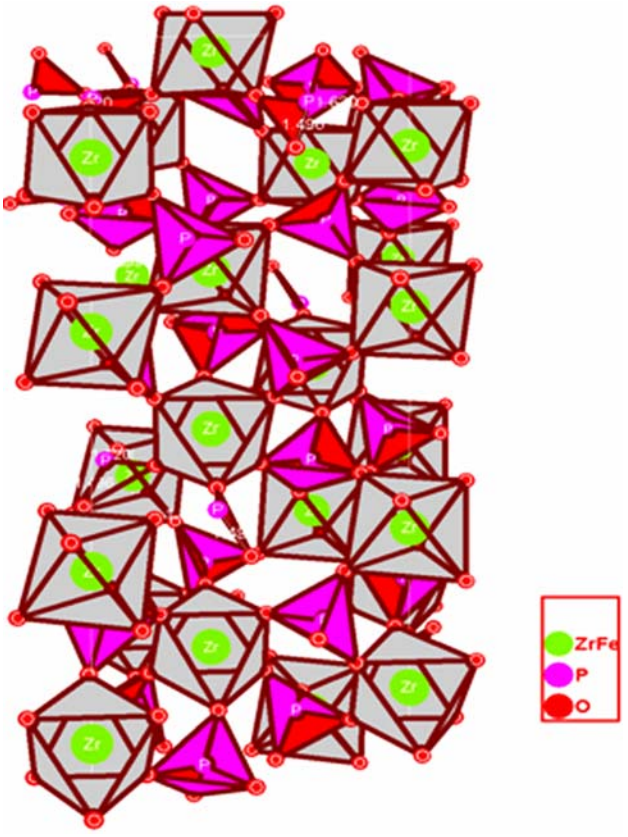

Fig. 4 Schematic representation of the polycrystalline $Na_{1.2}Zr_{1.8}Fe_{0.2}(PO_4)_3$. The structure showing the contacts between PO_4 tetrahedra and ZrO_6 octahedra

of electrons or electron holes). In an ideal solid electrolyte the former should be as large as possible and the later should be as low as possible. The electronic conductivity in unsubstituted NZP is low but on substitution for Zr or P with elements that can change valency, there is a possibility of creating free or quasi-free electrons. In the present investigation authors have found some electronic contribution to total conductivity, though significantly less than the ionic contribution. Analysis of AC conductivity data has been carried out by *complex plane* method which involves plotting the imaginary part Z'' against the real part Z'. When plotted on a linear scale, the data usually takes the form of a semicircle and/or spikes. The Z' and Z'' has been calculated by using well-known equations applicable to the LCR circuits [21]. The value of bulk resistance (R) may be determined from the intersection of either the spike or the semi circle with the Z' axis. The impedance plots (imaginary Z'' vs. real Z') have been recorded at different temperatures for the polycrystalline ceramic sample (Fig. 5). From these plots the overall resistance of the pellet at each temperature has been calculated and then the point wise conductivity values determined. The bulk conductivity values at room temperature are low in the order of 2.54×10^{-6} S cm^{-1}. However, a sharp increase (400 times) in bulk conductivity is seen with the rise in the temperature. At 500 °C the conductivity reaches a maximum of 1.11×10^{-3} S cm^{-1}. The plots of conductivity ($\log_{10}\sigma$) as functions of inverse temperature (1,000/T). The experimental data are well fitted to Arrhenius expressions, $\sigma = A \exp(-E_a/kT)$ for two

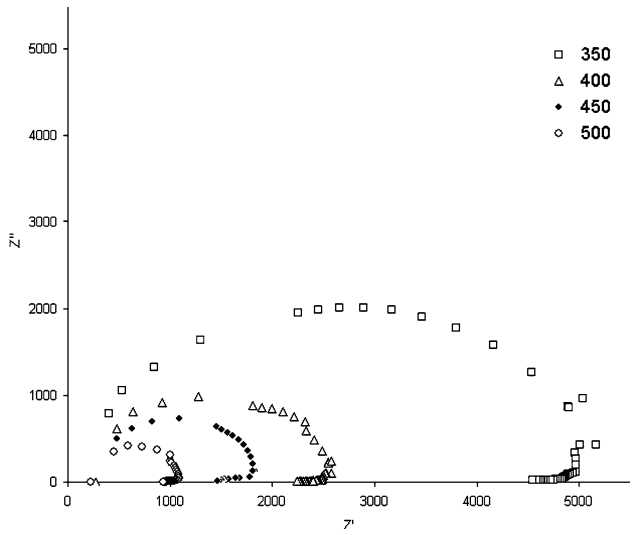

Fig. 5 High temperature complex impedance plots (imaginary Z'' vs. real Z') for polycrystalline $Na_{1.2}Zr_{1.8}Fe_{0.2}(PO_4)_3$

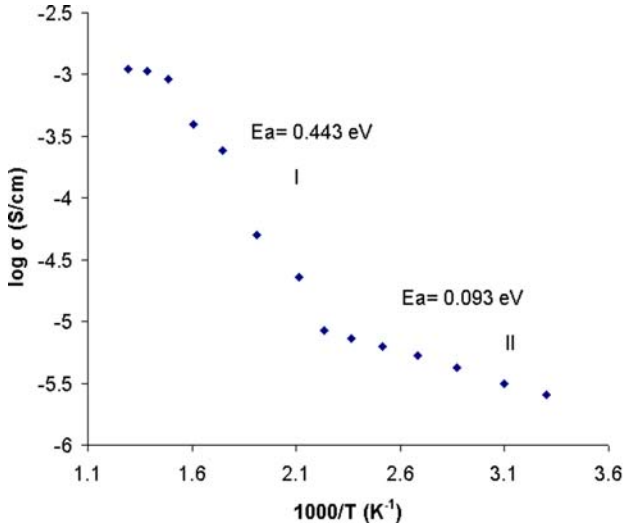

Fig. 6 Arrhenius plot of polycrystalline $Na_{1.2}Zr_{1.8}Fe_{0.2}(PO_4)_3$ investigated in the temperature range between 303 and 773 K. The Arrhenius plot shows marked change at 1,000/T of 2.23 (448 K)

different temperature segments where A is pre-exponential factor, which contains several constants including vibrational frequency of potentially mobile ion, E_a is the activation energies, k is the Boltzmann constant. The logarithmic plot consisting of two distinct segments I and II appears as combination of two straight lines with different slopes, below and above the transition temperature 448 K (1,000/T = 2.23) representing different thermal activation energies. Stages II and I correspond to regions of intrinsic and extrinsic conductivity respectively (Fig. 6). When the grains and grain boundary phase have almost the same sodium ionic conductivity, the resistances are in series and the largest thermal activation energy is observed at high temperature [22, 23]. The increase of activation energy above 448 K indicates either a new conduction mechanism or an increase of mobile species in the NZP structural framework at higher temperatures [24, 25]. In the intrinsic range the conductivity is a function of the product of sodium ion vacancy concentration and diffusion coefficient, each of them being an exponential function of temperature. On the other hand, at low temperature the concentration of sodium ion is not in thermal equilibrium but it is determined by minor solutes. This is the extrinsic range where temperature dependence of the conductivity is mostly a function of diffusion coefficient.

Conclusion

Refinement of powder X-ray diffraction data shows that the Fe substituted NZP crystallizes in the rhombohedral (R-3c space group) structure. The structure refinement suggests that Fe^{III} partially substitutes for zirconium via charge compensation being acquired by Na^+ in the structure. Crystal data and structural parameters of the material have been refined to a satisfactory convergence with reasonable values residual factors (R_p and R_{wp}). The calculated values of P–O and Zr–O bond lengths and O–M–O bond angles are in good agreement with the expected values. NZP appears to be a potential material for immobilization and solidification of iron from ILW. The material has been found to be of good structural integrity and also behaves as a good ionic conductor at elevated temperatures (573–773 K). The activation energy below and above the transition temperature (448 K) significantly differs in magnitude.

Acknowledgements We gratefully acknowledge the help of Dr Ranveer Kumar Department of Physics, Dr. H.S. Gour University for electrical measurements on the samples. The authors thank the University Grant Commission, New Delhi for funding the major project no. F-12-137/2001(SR-1) and to DST, New Delhi for providing X-ray facility at Jammu University.

Appendix 1

Table 4 O–M–O bond angles in polycrystalline $Na_{1.2}Zr_{1.8}Fe_{0.2}(PO_4)_3$

O6	Zr3	O6	95.5951(14)
O6	Zr3	O6	95.5951(14)
O6	Zr3	O7	90.7208(15)
O6	Zr3	O7	171.44920(10)
O6	Zr3	O7	89.5023(15)
O6	Zr3	O6	95.5951(14)
O6	Zr3	O7	89.5023(15)
O6	Zr3	O7	90.7208(15)
O6	Zr3	O7	171.44920(10)
O6	Zr3	O7	171.44920(10)
O6	Zr3	O7	89.5023(15)
O6	Zr3	O7	90.7208(15)
O7	Zr3	O7	83.5592(17)
O7	Zr3	O7	83.5592(17)
O7	Zr3	O7	83.5592(17)
O6	P5	O6	121.5751(19)
O6	P5	O7	100.0631
O6	P5	O7	112.4384(10)
O6	P5	O7	112.4383(10)
O6	P5	O7	100.0631
O7	P5	O7	110.493

Appendix 2

Table 5 Observed and calculated structure factors of polycrystalline phase $Na_{1.2}Zr_{1.8}Fe_{0.2}(PO_4)_3$

h	*k*	*l*	*d* space	Fosq	Fcsq	I_{100}
1	0	–2	6.32352	9.84E + 04	8.69E + 04	32.1274
1	0	–2	6.32352	1.23E + 05	8.69E + 04	27.9221
1	0	4	4.54872	5.14E + 05	5.39E + 05	92.1811
1	0	4	4.54872	5.47E + 05	5.39E + 05	68.3145
1	1	0	4.3979	5.77E + 05	5.58E + 05	97.649
1	1	0	4.3979	6.32E + 05	5.58E + 05	74.3971
1	1	3	3.8016	3.73E + 05	3.73E + 05	98.5186
1	1	3	3.8016	4.12E + 05	3.73E + 05	75.6122
2	0	–4	3.16176	8.84E + 05	8.49E + 05	86.5897
2	0	–4	3.16176	1.10E + 06	8.49E + 05	74.7915
1	1	6	2.86688	5.93E + 05	5.81E + 05	99.9999
1	1	6	2.86688	5.87E + 05	5.81E + 05	68.8776
2	1	1	2.85619	1.04E + 05	1.06E + 05	17.3421
2	1	1	2.85619	9.02E + 04	1.06E + 05	10.5181
2	1	4	2.56719	1.50E + 05	1.33E + 05	21.4649
2	1	4	2.56719	1.55E + 05	1.33E + 05	15.4709
3	0	0	2.53913	5.13E + 05	5.46E + 05	36.2403
3	0	0	2.53913	4.87E + 05	5.46E + 05	23.9699
2	0	8	2.27436	1.33E + 05	1.23E + 05	8.0916
2	0	8	2.27436	1.22E + 05	1.23E + 05	5.1576
1	1	9	2.18672	5.52E + 04	5.25E + 04	6.3725
1	1	9	2.18672	4.97E + 04	5.25E + 04	3.9951
3	0	–6	2.10784	2.24E + 05	1.99E + 05	12.321
3	0	–6	2.10784	1.71E + 05	1.99E + 05	6.5646
2	1	–8	2.0202	2.99E + 05	2.29E + 05	31.2413
2	1	–8	2.0202	2.25E + 05	2.29E + 05	16.3285
3	1	–4	1.97976	1.69E + 05	1.62E + 05	17.2123
3	1	–4	1.97976	1.32E + 05	1.62E + 05	9.3704
2	0	–10	1.94887	2.50E + 05	2.52E + 05	12.496
2	0	–10	1.94887	2.43E + 05	2.52E + 05	8.4471
2	2	6	1.9008	3.90E + 05	3.25E + 05	37.7956
2	2	6	1.9008	2.69E + 05	3.25E + 05	18.181
4	0	–2	1.87806	1.14E + 05	1.38E + 05	5.4425
2	1	10	1.78177	3.82E + 05	3.30E + 05	34.3006
2	1	10	1.78177	2.79E + 05	3.30E + 05	17.4303
3	1	–7	1.76977	6.90E + 04	6.30E + 04	6.1509
3	1	8	1.69412	1.48E + 05	1.03E + 05	12.5892
3	1	8	1.69412	1.03E + 05	1.03E + 05	6.0979
3	2	4	1.67005	2.23E + 05	1.66E + 05	18.6331
3	2	4	1.67005	1.91E + 05	1.66E + 05	11.0951
4	1	0	1.66225	3.14E + 05	2.87E + 05	26.0635
4	1	0	1.66225	2.08E + 05	2.87E + 05	12.0291
1	0	–14	1.58478	2.16E + 05	1.47E + 05	8.5233
1	0	–14	1.58478	1.75E + 05	1.47E + 05	4.8154
4	0	–8	1.58088	1.70E + 05	1.41E + 05	6.7022
3	1	–10	1.54599	2.59E + 05	2.21E + 05	19.8718
3	1	–10	1.54599	1.64E + 05	2.21E + 05	8.7685
4	1	–6	1.52166	1.31E + 05	8.82E + 04	9.9295
4	1	6	1.52166	1.46E + 05	9.75E + 04	10.9942
2	0	14	1.49093	3.35E + 05	3.21E + 05	12.3739
2	0	14	1.49093	2.74E + 05	3.21E + 05	7.0542
5	0	–4	1.47131	1.85E + 05	1.28E + 05	6.7537
4	0	10	1.4585	1.87E + 05	1.96E + 05	6.7607
3	3	0	1.46597	1.55E + 05	1.43E + 05	5.6419
2	1	–14	1.412	1.86E + 05	1.28E + 05	12.992
2	1	–14	1.412	1.05E + 05	1.28E + 05	5.0971
4	2	–4	1.3953	7.81E + 04	5.74E + 04	5.3987
3	2	10	1.38436	8.19E + 04	6.69E + 04	5.6097

The seven columns within each group contain the values *h*, *k*, *l*, *d* spacing, structure factor Fosq (observed), Fcsq (calculated) and intensity, respectively. The reflection selected from the CIF output of the final cycle of the refinement

References

1. Scheetz BE, Agrawal DK, Brevel E, Roy R (1994) Sodium zirconium phosphate (NZP) as a host structure for Nuclear waste immobilization: a review. Waste Management 14(6):489
2. Breval E, Agrawal DK (1995) Brit Ceram Trans 94:27
3. Orlova AI, Pet'kov VI, Skiba OV (1997) In: International conference on future nuclear system, Global '97, Yokohama Proceedings, vol 2. p 1253
4. Hazen RM, Prewitt CT (1977) Am Mineral 62:309
5. Govindan Kutty KV, Asuvathraman R, Sridhran R (1998) J Mat Sci 33:4007
6. Kohler J, Imanaka N, Adachi G (1999) Chem Mater 10:1767
7. Verissimo Carla MS, Garrido Francisco L, Oswaldo A, Paloma C, Ana M-J, Iglesias Juan E, Rojo Jose M (1997) Solid State Ionics 100:127
8. Roy R, Agrawal DK, Alammo J, Roy RA (1984) Mat Res Bull 19:471
9. Hirose Y, Fukasawa T, Agrawal DK, Scheetz BE, Nageswaran R, Curtis JA, Limaye SY (1999) In: WM 1999 conference
10. Shannon RD (1976) Acta Crystallogr A 32:751
11. Goodenough JB, Hong HYP, Kafalas JA (1976) Mat Res Bull 11:203
12. Hagman L, Kierkegaard P (1968) Acta Chem Stand 22:1822
13. Hong HYP (1976) Mat Res Bull 11:173
14. Pet'kov VI, Orlova AI, Kazantsev GN, Samoilov SG, Spiridonova ML (2001) J Therm Anal Calorimetr 66:623
15. Buvaneswaria G, Govindan Kutty KV, Varadaraju UV (2004) Mat Res Bull 39:475
16. JCPDS Powder diffraction data file no. 71-0959 (2000) Compiled by International Center for Diffraction Data USA
17. Larson AC, Von Dreele RB, General structure analysis system technical manual, LANSCE, MS-H805, Los Alamos National Laboratory, USA
18. Furberg S (1955) Acta Chem Scand 9:1557
19. Cruickshank DWJ (1964) Acta Cryst 17:671
20. Nord AG, Kiekegaard P (1968) Acta Chem Scand 22:1465
21. West AR (1998) Solid state chemistry and its application, John Willey, New York, pp 484–487
22. Breval E, McKinstry HA, Agrawal DK (1994) Br Ceram Trans 93(6):239
23. Nowick AS, LeeWK (1989) In: Laksar AL, Chandra S (eds) Superionic solids and solid electrolytes, recent trends. Academic press, Boston pp 381–405
24. Le Meins JM, Bohnke O, Gourbion G (1998) Solid State Ionics 111:67
25. Tilement O, Angenaut J, Couturier JC, Quarton M (1991) Solid State Ionics 44:299